

# Inelastic Collision Rates of Trapped Metastable Hydrogen

David Landhuis,\* Lia Matos, Stephen C. Moss, Julia K. Steinberger, Kendra Vant,  
Lorenz Willmann,† Thomas J. Gretyak, and Daniel Kleppner

*Department of Physics and Center for Ultracold Atoms,  
Massachusetts Institute of Technology, Cambridge, Massachusetts 02139*  
(November 15, 2018)

## Abstract

We report the first detailed decay studies of trapped metastable ( $2S$ ) hydrogen. By two-photon excitation of ultracold H samples, we have produced clouds of at least  $5 \times 10^7$  magnetically trapped  $2S$  atoms at densities greater than  $4 \times 10^{10} \text{ cm}^{-3}$  and temperatures below  $100 \mu\text{K}$ . At these densities and temperatures, two-body inelastic collisions of metastables are evident. Experimental values for the total two-body loss rate constant are  $K_2 = 1.8_{-0.7}^{+1.8} \times 10^{-9} \text{ cm}^3/\text{s}$  at  $87 \mu\text{K}$  and  $K_2 = 1.0_{-0.5}^{+0.9} \times 10^{-9} \text{ cm}^3/\text{s}$  at  $230 \mu\text{K}$ . These results are in the range of recent theoretical calculations for the total  $2S$ - $2S$  inelastic rate constant. The metastable clouds were excited in a gas of ground state ( $1S$ ) hydrogen with peak densities reaching  $7 \times 10^{13} \text{ cm}^{-3}$ . From the one-body component of the metastable decay, we derive experimental upper limits for  $K_{12}$ , the rate constant for loss due to inelastic  $1S$ - $2S$  collisions.

## I. INTRODUCTION

The ability to create large clouds of metastable ( $2S$ ) H atoms in a magnetic trap makes it possible to study the rich collisional physics of cold metastable H. In an encounter between two metastables, the possible outcomes include Penning ionization, the formation of molecular ions, excitation transfer to short-lived  $2P$  states, and hyperfine transitions [1,2]. If the  $2S$  atoms are generated from a background  $1S$  gas, then several  $1S$ - $2S$  collision processes may also occur. Though these states of H are among the simplest atomic states in nature, an accurate description of their inelastic collisions at low energies remains a theoretical challenge [1,3,4].

At low temperatures, the rate of quenching collisions between metastables is small enough to allow dense ( $> 10^{10} \text{ cm}^{-3}$ )  $2S$  clouds to exist for tens of milliseconds, which is an appreciable fraction of the 122 ms natural lifetime of the  $2S$  state. Such a cloud can serve as an atom source for precision spectroscopy of transitions originating in the  $2S$  state. In particular, the absolute frequencies of transitions from the  $2S$  to higher-lying states can be combined with the well-known  $1S$ - $2S$  interval to simultaneously determine the  $1S$  Lamb shift (a sensitive test of QED) and the Rydberg constant (which relates several more fundamental constants) [5–7]. Taking advantage of the high signal-to-noise ratio possible in a cold, trapped sample, spectroscopy of metastable H may lead to a significant advance in accuracy for the determination of these quantities [8].

Cold metastable H is also potentially interesting for “quantum atom optics” experiments involving single-atom detection. The large (10 eV) internal energy of a  $2S$  atom is easily registered by an ionizing collision on an electron-multiplying detector, or by detecting the Lyman- $\alpha$  photon emitted at a surface or other localized electric field. As demonstrated already with metastable noble gases, single-atom detection allows experiments involving atom-atom correlations, atom interferometry, or atom holography [9–11]. A metastable beam ejected from a trapped H sample, potentially much brighter than other cold metastable beams to date, may be a useful source for quantum atom optics research.

After improving our apparatus at MIT, we have been able to generate metastable H clouds which are larger and longer-lived than in our previous work [12,13]. In this paper, we report results from decay studies of trapped  $2S$  clouds, conducted at temperatures ranging from a few mK to below 100  $\mu\text{K}$ . These results include the first experimental determinations of the  $2S$ - $2S$  two-body loss rate constant  $K_2$  and upper limits for the  $1S$ - $2S$  inelastic rate constant  $K_{12}$ . In the case of  $K_2$ , we have observed a temperature dependence below 230  $\mu\text{K}$  which is not predicted in the current theory for cold metastable H collisions [14]. This work serves as a stepping stone to high-resolution spectroscopy experiments which probe fundamental physics. Knowledge of metastable collision parameters may also be instrumental in the development of single-atom detection experiments involving H.

## II. EXPERIMENTAL METHODS

The methods we use for trapping and cooling atomic H in a cryogenic apparatus (Fig. 1(a)) are described elsewhere [13,15,16]. Molecular hydrogen is dissociated in a discharge chamber that is thermally anchored at one end to a dilution refrigerator and opens to a trapping cell at the other end. Atoms in the  $F = 1$ ,  $m_F = 1$  hyperfine state of the  $1S$

manifold are captured in a Ioffe-Pritchard magnetic trap [17], initially 500 mK deep. With typical aspect ratios between 100:1 and 400:1, the cloud is shaped like a highly elongated ellipsoid, cylindrically symmetric about the trap axis. We refer to the direction along the trap axis as “axial” and to the perpendicular direction as “radial.”

If an atom has sufficient energy, it can escape over a magnetic field saddlepoint located at one end of the trap. The sample can be cooled to a temperature of  $\sim 200 \mu\text{K}$  by progressively lowering the saddlepoint field, thus forcing evaporation [18]. If further cooling is desired, rf-induced evaporation is employed to reach temperatures as low as  $\sim 20 \mu\text{K}$  [19]. The number of atoms in the trap ranges from more than  $10^{14}$  after initial loading to  $\sim 10^{10}$  at the lowest temperatures. For the experiments described in this paper, the samples were not Bose degenerate, and typical peak  $1S$  densities ranged from  $10^{13} \text{ cm}^{-3}$  to  $10^{14} \text{ cm}^{-3}$ .

To generate metastable hydrogen, we excite the two-photon  $1S$ - $2S$  transition with a 243 nm laser [12]. To achieve large excitation rates, typically  $\sim 15 \text{ mW}$  of laser power is focused to a radius of  $\sim 20 \mu\text{m}$  near the trap minimum. In accordance with the two-photon selection rules, the metastables produced are in the  $F = 1$ ,  $m_F = 1$  state of the  $2S$  manifold; except for a small relativistic correction ( $\sim 10^{-4}$ ), these experience the same magnetic trapping potential as the  $1S$  atoms. In the presence of a weak electric field of strength  $E$ , the  $2S$  state quenches at a rate  $\gamma_s = 2800E^2 (\text{cm}^2/\text{V}^2)\text{s}^{-1}$  due to Stark-mixing with the  $2P$  state [20]. To detect the metastables, a field of 10 V/cm is applied, quenching the  $2S$  atoms in a few microseconds. A small fraction of the resulting 122 nm Lyman- $\alpha$  photons are counted on a microchannel plate (MCP) detector. The metastable decay behavior is observed by cycling through a series of different wait times between excitation and quench pulses (Fig. 1(b)). During the trap lifetime of the ground state sample, typically several minutes, we can make many  $2S$  decay measurements. Samples of differing initial  $2S$  density are obtained by stepping the laser frequency across the resonance.

For the measurements discussed here, the detection efficiency was approximately  $2 \times 10^{-6}$ . This was calibrated using a  $230 \mu\text{K}$  sample where the initial number of  $1S$  atoms was known from bolometric density measurements [13] and the trap geometry. The sample was depleted by resonant  $1S$ - $2S$  excitation and subsequent quenching to an untrapped state. With appropriate corrections, the detection efficiency can be inferred from the total number of signal photons counted and the initial number of atoms [21]. The corrections account for other loss mechanisms, for the branching ratio back to the trapped ground state, and for reabsorption (“radiation trapping”) of the Lyman- $\alpha$  photons by the ground state cloud. The photons emitted by the quenched metastables have a frequency which is detuned from a 100 MHz-wide  $1S$ - $2P$  absorption resonance by only 1.1 GHz, and at the densities achieved in our experiments, the effects of radiation trapping are significant. Using Monte Carlo simulations of Lyman- $\alpha$  propagation in experimentally realistic cloud geometries, it was determined that typically  $\sim 30\%$  of potential signal photons are absorbed and scattered in the atom cloud [21]. Other factors, such as the small detection solid angle ( $1.1 \times 10^{-2} \text{ sr}$ ), the transmission of two  $\text{MgF}_2$  windows between the atoms and the MCP, and the MCP quantum efficiency, lead to the small overall detection efficiency.

Based on the detection efficiency, we can estimate  $N_{2S}$ , the population of the metastable cloud, and  $n_{2S}$ , the peak metastable density in the trap. In a very cold sample ( $87 \mu\text{K}$ ), as many as 150 Lyman- $\alpha$  photons were observed on the MCP after a single laser shot, implying  $N_{2S} \simeq 8 \times 10^7$ . The effective volume,  $V_{2S} = N_{2S}/n_{2S}$ , of the metastable clouds for these

samples is  $\sim 1 \times 10^{-3} \text{ cm}^3$ , which means that densities of  $\sim 10^{11} \text{ cm}^{-3}$  have been achieved.

Due to scatter from optics inside the trapping cell, each laser pulse induces some background fluorescence which is detected with low efficiency at the MCP. The background, which is typically small compared to the metastable signal, decays in a few milliseconds to a negligible level. To establish a background correction for our decay data, the laser is tuned far off resonance at the end of each trapping sequence. The background fluorescence is then recorded for the same cycle of wait times used when generating metastables.

In earlier experiments, performed in an entirely nonmetallic cell, we found that stray electric fields limited metastable lifetimes to 1 ms or less. In the current version of the apparatus, a copper film has been added to the inside surface of the trapping cell. The film is thin enough to allow rf to penetrate the trapping cell from outside coils, yet thick enough to significantly suppress stray dc fields. As depicted in Fig. 2(a), the copper film has been divided into several contiguous electrodes which are used to apply both the quench pulses and a compensating dc field. The dc voltage which best compensates for stray fields is found by measuring the metastable decay rate in a low density sample for several applied voltages. As shown in Fig. 2(b), we observe the expected quadratic dependence of the decay rate on electric field. With optimal stray field compensation, metastable lifetimes as long as 100 ms have been observed, approaching the natural lifetime of the  $2S$  state.

Our decay measurements have focused on metastable clouds generated in four magnetic trap configurations, spanning a range of temperatures and ground state densities. These trap configurations are designated Traps W, X, Y, and Z, and each has its own standard evaporation sequence for sample preparation. To increase the signal-to-noise ratio, decay measurements were repeated in each trap over several consecutive trap cycles.

Densities and temperatures of the standard samples and the approximate trajectories by which they were created are depicted in Fig. 3 [21]. To ensure that the colder samples (W, X, and Y) had reached thermal equilibrium, they were held undisturbed for 30 s after the end of the forced evaporation. The sample densities were measured to 20% accuracy by the bolometric method [13], and the temperatures were determined by a combination of methods. For the coldest sample (W), the temperature was calibrated to within 5% by measuring the width of the Doppler-sensitive  $1S$ - $2S$  line [16]. The temperature of Trap X was determined by comparing the widths of the Doppler-free  $1S$ - $2S$  resonances of Traps W and X in the low density limit [12]. For Traps Y and Z, the temperature was established using results from a numerical simulation of evaporative cooling [22]. The temperature uncertainty for Traps X, Y, and Z is estimated to be 10%.

### III. EVIDENCE FOR $2S$ - $2S$ TWO-BODY LOSS

Our investigation of inelastic  $2S$ - $2S$  collisions was initiated by observations of how the decay behavior depended on metastable density. In each of the standard traps the  $2S$  density was varied by generating metastables at different laser detunings and also by exciting different  $1S$  densities as the ground state sample decayed. The decay curves were binned according to the total number of metastable signal counts in each decay curve. Since, to a first approximation, the signal is proportional to the metastable density, this means that decay curves corresponding to approximately the same initial  $2S$  density were averaged together. For a preliminary analysis, the average decay curves were fit to a simple exponential

function, with only the decay rate and initial amplitude as free parameters. Figure 4 shows the results of this analysis. In the two coldest traps, W and X, the decay rate clearly increases with increasing metastable density, consistent with the presence of two-body inelastic loss processes. Furthermore, among the four traps, the decay rate is largest in Trap W, where the highest metastable densities are achieved.

The peak  $2S$  densities achieved in each trap can be estimated from the number of signal counts observed, but the uncertainty is large, reflecting significant uncertainties in both the metastable cloud shape and the detection efficiency. The shape of the  $2S$  cloud depends sensitively on the location of the laser beam waists with respect to the magnetic trap. For the density values listed in Fig. 4, a detection efficiency of  $2 \times 10^{-6}$  was assumed, and the counterpropagating laser beams were assumed to be perfectly overlapped and well-aligned with the atom cloud; with a plausible misalignment, the actual densities could be a factor of 3 smaller.

As illustrated in Fig. 5, a comparison of the average decay curves at high and low metastable signal provides further evidence for two-body loss at high densities. At low  $2S$  densities, the decay curves are well described by an exponential decay. By contrast, the decay curves at high  $2S$  densities deviate significantly from a simple exponential. They are better fit by a “one-plus-two” model with a free two-body decay parameter and a one-body decay rate fixed at its low density value. The one-plus-two model is described further in Sec. IV.

In principle, three-body inelastic collisions could also contribute to the observed density dependence of the decay. However, the three-body loss rate constant for metastables would have to be unexpectedly large to play a significant role at our experimental densities ( $\lesssim 10^{11} \text{ cm}^{-3}$ ) [23]. In the following analysis, we assume that two-body effects dominate.

#### IV. DETERMINATION OF THE TWO-BODY LOSS RATE CONSTANT

In this section, we derive the rate constant  $K_2$  for two-body loss of metastables based on decay data of the form  $s(t)$ , the number of signal counts observed when quenching at wait time  $t$ . The constant is defined as follows to give the rate of change of the local  $2S$  density  $n_{2S}(\mathbf{r})$  due to two-body processes:

$$\dot{n}_{2S}(\mathbf{r}) \Big|_{\text{two-body}} = -K_2 n_{2S}^2(\mathbf{r}). \quad (1)$$

If the relative distribution of metastables in the trap is not changing in time (“static approximation”),  $K_2$  is the product of the metastable detection efficiency, a factor describing the cloud geometry, and a two-body decay parameter extracted from fits to  $s(t)$ . After analyzing the decay process in the static approximation, we introduce dynamic corrections to obtain final results for  $K_2$ .

Given the geometry of our apparatus and the ground state densities achieved, it is a reasonable first approximation to assume that the metastable cloud does not change shape as it decays. The initial extent of the metastable cloud along the trap axis, about 2 cm between the  $1/e$  points, is defined by the depth of focus of the laser. This is shorter than the thermal length of the ground state cloud, which ranges from 4 cm in Trap W to 23 cm in Trap Z. On the time scale of the decay, the  $2S$  atoms collide frequently with  $1S$  atoms. At

the peak ground state density in Trap W, for example, the  $2S$  mean free path is  $100 \mu\text{m}$ , and the mean time between collisions is  $70 \mu\text{s}$ . (To calculate these values, we use the theoretical value for  $a_{1S-2S}$ , the elastic  $1S$ - $2S$  scattering length [24].) Thus, the metastables diffuse slowly along the trap axis. Numerical simulations of the time evolution of the  $2S$  cloud have shown that over a cloud lifetime of  $100 \text{ ms}$ , the shape of the initial axial distribution does not change dramatically [21]. In the radial direction, the cloud shape evolves even less, although for a different reason. Due to the geometry of the magnetic trap, the metastable cloud is cylindrically symmetric and confined to the same thermal radius as the ground state cloud. This thermal radius, about  $110 \mu\text{m}$  for Trap W, is comparable to the  $2S$  mean free path. In a time shorter than the  $2 \text{ ms}$  excitation pulse, the metastables establish an equilibrium spatial distribution across the short radial dimension. The relative spatial distribution of metastables is quasi-static, then, because (1) axial diffusion through the  $1S$  gas is slow and (2) radial equilibrium exists over the lifetime of the  $2S$  cloud.

In the static approximation, the rate of signal decay can be described by the differential equation

$$\dot{s} = -\alpha_1 s - \alpha_2 s^2, \quad (2)$$

where  $\alpha_1$  and  $\alpha_2$  are, respectively, parameters corresponding to one- and two-body decay. The solution to Eq. 2 is

$$s(t) = \frac{\alpha_1 A_o e^{-\alpha_1 t}}{\alpha_1 + \alpha_2 A_o (1 - e^{-\alpha_1 t})}, \quad (3)$$

which we have named the “one-plus-two” model. The parameter  $\alpha_1$  is the one-body decay rate, the total rate of decay due to processes which are independent of  $2S$  density. Contributions to the one-body rate include the natural decay of the  $2S$  state, quenching due to stray electric fields, and inelastic collisions with the background  $1S$  gas.

For a decay measurement with a very high signal-to-noise ratio, one could extract  $\alpha_1$ ,  $\alpha_2$ , and  $A_o$  simultaneously by a fit to the “one-plus-two” model. The parameters  $\alpha_1$  and  $\alpha_2$  are highly correlated, however. With the modest signal-to-noise ratio in our data, a consistent convergence of the fit is not assured. Thus, we employ an alternate method of analysis. For a given trap and  $1S$  density, the value for  $\alpha_1$  is determined by extrapolating the best-fitting exponential decay rates to zero metastable density (Fig. 6). This leaves two free parameters in the one-plus-two model:  $A_o$ , the signal which would be observed at  $t = 0$ , and  $\alpha_2$ , from which  $K_2$  can be calculated.

By integrating Eq. 1 over the entire trap, we obtain an expression for the total number of metastables lost per unit time due to two-body processes:

$$\dot{N}_{2S} \Big|_{\text{two-body}} = -K_2 n_{o,2S}^2 \int f_{2S}^2(\mathbf{r}) d^3\mathbf{r}. \quad (4)$$

Here,  $N_{2S}$  is the number of  $2S$  atoms in the trap, and  $f_{2S}(\mathbf{r}) = n_{2S}(\mathbf{r})/n_{o,2S}$  is the normalized spatial distribution function for metastables, where  $n_{o,2S}$  is the peak  $2S$  density. Since  $s = \epsilon N_{2S}$ , where  $\epsilon$  is the detection efficiency, and since

$$\dot{s} \Big|_{\text{two-body}} = -\alpha_2 s^2, \quad (5)$$

it follows that

$$K_2 = \zeta \epsilon \alpha_2 \quad (6)$$

in the static approximation, where  $\zeta$  is a geometry factor defined by

$$\zeta = \frac{\int f_{2S}^2(\mathbf{r}) d^3\mathbf{r}}{\left[\int f_{2S}(\mathbf{r}) d^3\mathbf{r}\right]^2}. \quad (7)$$

To obtain Eq. 6, we have used the fact that  $n_{o,2S} = N_{2S} / \int f_{2S}(\mathbf{r}) d^3\mathbf{r}$ . The quantity  $\zeta$ , which has units of volume, is a measure of the spatial extent of the metastable cloud;  $\zeta$  decreases as  $f_{2S}(\mathbf{r})$  becomes more sharply peaked.

Thus to determine  $K_2$  from our decay data it is necessary to know  $\epsilon$  and the shape of the metastable cloud. Our method for determining  $\epsilon$  was described in Sec. II. To calculate  $\zeta$  for various trap configurations and temperatures, we employed a Monte Carlo simulation of  $1S$ - $2S$  excitation in our trap [25]. The simulation calculates the excitation lineshape associated with atoms in a volume slice perpendicular to the trap axis. In addition to the position of the volume slice along the axis, the inputs to the simulation include the laser field geometry, the laser pulse length, the trap shape, the sample temperature, and the peak  $1S$  density. The lineshape is calculated by choosing atoms randomly from a thermal distribution, computing their trajectories during the laser pulse, and then finding the contribution of each atom to the spectrum by Fourier-transforming the time-varying laser field amplitude seen by the atom. The effects of the  $1S$ - $2S$  cold collision shift [13] are incorporated by allowing the resonance frequency to vary over the trajectory in accordance with the local  $1S$  density. After repeating the lineshape calculation for many slices covering the length of the  $2S$  cloud along the trap axis, the axial distribution of metastables at  $t = 0$  can be extracted for any given laser detuning. Under the assumption that the metastables establish an equilibrium radial distribution during the pulse,  $f_{2S}(\mathbf{r})$  for the entire trap is easily calculated from the axial distribution.

An additional numerical calculation corrects the lineshape simulation results to account for photoionization, the promotion of  $2S$  electrons to the continuum by the excitation laser. In a cold, dense sample, such as those prepared in Trap W, the metastables spend a relatively long time in the high-intensity UV laser field, and the fraction of metastables lost to photoionization can exceed 30% [21].

Because the lineshape simulation has given results in good agreement with experimental  $1S$ - $2S$  spectra for a wide range of trap shapes, densities, and temperatures, this method of calculating  $f_{2S}(\mathbf{r})$  is believed reliable. For each spatial distribution function,  $\zeta$  is computed by numerical evaluation of Eq. 7. Values for  $\zeta$  range from approximately  $2 \times 10^{-3} \text{ cm}^3$  in Trap W to  $0.2 \text{ cm}^3$  in Trap Z. Depending on the laser detuning, an imperfect overlap of the counterpropagating laser beam focuses along the trap axis may cause  $\zeta$  to be 50-100% larger. Uncertainty in the knowledge of the laser field geometry is the principal source of uncertainty in  $\zeta$ .

The experimental results for  $K_2$ , calculated on the basis of Eq. 6, are listed in the “static approximation” column of Table I. For each standard trap, the accumulated decay curves were binned together according to laser detuning, and the resulting average curves were fit with the one-plus-two model to obtain  $\alpha_2$  as a function of detuning. Next, the values for  $\alpha_2$

were multiplied by the detection efficiency and the value of  $\zeta$  appropriate for the detuning. The resulting values for  $K_2$  were found to be largely independent of laser detuning, indicating that variations in metastable cloud shape with detuning are reasonably accounted for by our lineshape simulation. For Traps W and X, the weighted averages across all detunings are reported in Table I. In the warmer samples, where the  $2S$  density is too low to observe two-body collisions, the weighted average for  $K_2$  is consistent with zero. For these, Table I reports upper limits for  $K_2$  based on linear addition of the uncertainties in  $\alpha_2$ ,  $\epsilon$ , and  $\zeta$ .

The error bars for Traps W and X are primarily due to systematic uncertainties. These errors are asymmetric due to asymmetric uncertainty in the detection efficiency and the fact that laser misalignments generally increase  $\zeta$ . The most important contributions to the overall error in  $K_2$  come from the detection efficiency and uncertainty in the axial overlap of the laser focuses. In Trap W, for example,  $\epsilon = 1.8 \times 10^{-6}$  with approximate relative uncertainties of 30% on the lower side and 60% on the upper side. The focus overlap uncertainty contributes 75% to the upper relative error. Other sources of uncertainty include the error in the determination of  $\alpha_2$  ( $\pm 12\%$ ) and contributions of a few percent each due to uncertainties in the beam radius, cold collision shift parameter, offset of the trap minimum and laser focuses, ground state density, and sample temperature. With some minor exceptions, the various uncertainties are assumed to be uncorrelated, and the relative errors we report for  $K_2$  are essentially quadrature sums of the contributing errors.

The static approximation results need to be refined to account for change in the metastable spatial distribution while the cloud decays. There is a flattening of the initial axial distribution due to diffusion and to two-body loss, which occurs preferentially where the  $2S$  density is highest. This flattening of the distribution in time causes the initial decay of the metastable population to be somewhat less steep than it would be if the cloud shape were completely static. Thus, the value of  $\alpha_2$  determined by fitting a decay curve to the one-plus-two model is smaller than the effective value of  $\alpha_2$  which accounts for dynamics when substituted into Eq. 6.

To calculate corrections to the static approximation analysis, a numerical simulation of the decaying metastable cloud was developed. For each standard sample, the simulation was repeated many times assuming different laser detunings. The starting point for each simulation run was a cloud with distribution  $f_{2S}(\mathbf{r})$ , calculated by the method described above, and an initial total number of metastables  $N_{2S}(0) = A_o/\epsilon$ , where  $A_o = s(0)$  was determined from experimental data. The simulation then evolved both dynamic and static clouds forward in time from the initial condition. For the dynamic cloud, the axial distribution was adjusted locally at each time step for losses due to one-body processes (parametrized by  $\alpha_1$ ), two-body processes (parametrized by a putative value for  $K_2$ ), and for diffusion of  $2S$  atoms in the  $1S$  background. For the static cloud,  $N_{2S}$  was adjusted at each time step for one- and two-body losses integrated over the whole cloud, but the spatial distribution remained fixed. After evolving the clouds over 100 ms, the simulated static and dynamic metastable decay curves were fit by the one-plus-two model. The ratio  $\alpha_{2,\text{static}}/\alpha_{2,\text{dynamic}}$  from the simulation was used as a correction factor for the experimentally determined  $\alpha_2$  values. New average values for  $K_2$  were then calculated for each trap. It was found that the static approximation values of  $K_2$  must be multiplied by 1.35 and 1.30, respectively, to correct for dynamics in Traps W and X. By varying the inputs to the decay simulation, the uncertainty in the overall correction factors was estimated to be 10%. For Traps Y and Z, a conservative upper limit

for the correction factor is 2. The final results for  $K_2$  are summarized in the last column of Table I.

Theoretical  $2S$ - $2S$  collision rates at low temperatures were calculated recently by Forrey and collaborators [14], extending their previous work for high temperatures [1]. The calculations indicate that the most prevalent inelastic process in a cold metastable cloud is double excitation transfer,  $H(2S) + H(2S) \rightarrow H(2P) + H(2P)$ . Next in importance are the two possible ionization processes: associative ionization, in which the molecular ion  $H_2^+$  is formed, and Penning ionization, where the internal energy of one metastable atom causes the ionization of a second metastable. Since processes involving  $2S$  hyperfine state changes are mediated by comparatively weak magnetic dipole interactions, they are expected to be negligible in relation to excitation transfer and ionization. Thus, a theoretical estimate for  $K_2$  is obtained by summing the loss rate constants for double excitation transfer and ionization. For each process, the loss rate constant equals  $2\langle\sigma v\rangle$ , where  $\sigma$  is the cross section for the process,  $v$  is the relative velocity of two atoms, the angle brackets indicate a thermal average, and the factor of 2 accounts for the fact that two metastables are lost in each collision. The theoretical curve for  $K_2$  as a function of temperature is shown alongside the experimental values in Fig. 7.

The uncertainty in the theoretical results is difficult to estimate. In its current state of development, the theory for  $2S$ - $2S$  collisions neglects hyperfine structure and assumes zero coupling between the relative orbital angular momentum of the nuclei and the angular momentum of the electrons. It is not yet certain whether this assumption is justified for spin-polarized metastables at low temperatures [23]. Furthermore, the theory calculations assume zero magnetic field, while in the experiment the trapped metastables experience a field of a few gauss. Nevertheless, from Fig. 7 we can conclude that the present theory correctly predicts  $K_2$  at low temperatures to within an order of magnitude.

An intriguing aspect of the experimental results for  $K_2$  is the apparent temperature dependence between  $87 \mu\text{K}$  and  $230 \mu\text{K}$ . Although the absolute uncertainty is large for each temperature point, we believe that the temperature dependence is real. The error bars are primarily due to systematic uncertainties which affect both points in approximately the same way. When the correlated errors are removed, the ratio of  $K_2$  at  $87 \mu\text{K}$  to  $K_2$  at  $230 \mu\text{K}$  is found to be  $1.9 \pm 0.4$ . This result contrasts with the theoretical prediction that  $K_2$  is virtually independent of temperature in this regime, consistent with Wigner threshold behavior. Further theoretical and experimental work will be necessary to understand the temperature dependence of inelastic  $2S$ - $2S$  collisions near  $T = 0$ .

## V. UPPER LIMIT FOR THE $1S$ - $2S$ LOSS RATE CONSTANT

In addition to the two-body loss channels discussed above, metastables are lost from the trap by several one-body mechanisms. These include the natural decay of the  $2S$  state by spontaneous emission of two photons, quenching due to stray electric fields, and loss due to inelastic  $1S$ - $2S$  collisions. In a collision with a ground state atom, a metastable may be lost by a transition to either an untrapped  $2S$  state (hyperfine-changing collision) or to a  $2P$  state (excitation transfer). If inelastic  $1S$ - $2S$  collisions are sufficiently probable, they should result in a dependence of the observed one-body decay parameter  $\alpha_1$  on the peak ground state density  $n_{1S,o}$ .

To search for evidence of inelastic  $1S$ - $2S$  collisions, the decay curves taken in the standard trap configurations were organized into consecutive time bins of 9.6 s duration. Next, a value for  $\alpha_1$  was determined for each bin by extrapolating the decay rate to zero metastable signal, as in Fig. 6. Then, for each trap,  $\alpha_1$  was plotted as a function of time over the 120 s period following initial preparation of the sample (see Fig. 8(a), for example). During this time, the ground state density decays significantly due to  $1S$ - $1S$  dipolar decay (Fig. 8(b)).

As shown in Fig. 8, the data suggests that some component of one-body loss decreases as the ground state density decreases. However, since the trend is not large relative to uncertainties, it is inconclusive whether significant loss due to  $1S$ - $2S$  collisions exists in our metastable clouds. We have not attempted to fit the time (or density) dependence of  $\alpha_1$  to a model but instead have determined conservative upper limits for the metastable loss rate due to collisions with the ground state background.

An upper limit on the total inelastic contribution  $\alpha_{1,\text{inel}}$  to the one-body decay rate is found by subtracting the natural decay rate ( $\gamma_{\text{nat}} = 8.2 \text{ s}^{-1}$ ) from the total one-body decay rate:

$$\alpha_{1,\text{inel}} < \alpha_1 - \gamma_{\text{nat}}. \quad (8)$$

Analogous to Eq. 1, we define a rate constant  $K_{12}$  for the metastable loss rate due to inelastic  $1S$ - $2S$  collisions, such that

$$\dot{n}_{2S}(\mathbf{r}) \Big|_{1S-2S} = -K_{12} n_{1S}(\mathbf{r}) n_{2S}(\mathbf{r}). \quad (9)$$

Using a static approximation for the metastable cloud, Eq. 9 can be integrated over the entire trap to find the relation between  $K_{12}$  and  $\alpha_{1,\text{inel}}$ :

$$K_{12} = \frac{\alpha_{1,\text{inel}} V_{2S}}{n_{1S,o} Q_{12}}, \quad (10)$$

where  $V_{2S} = \int f_{2S}(\mathbf{r}) d^3\mathbf{r}$ , and  $Q_{12} = \int f_{1S}(\mathbf{r}) f_{2S}(\mathbf{r}) d^3\mathbf{r}$ . By combining an experimental upper limit for the initial value of  $\alpha_{1,\text{inel}}$  in each trap, a numerically computed upper limit for the ratio  $V_{2S}/Q_{12}$ , and the measured peak density, we have obtained the upper limits on  $K_{12}$  listed in Table II.

These upper limits are much larger than the theoretical rate constant for  $1S$ - $1S$  dipolar decay,  $g = 1.2 \times 10^{-15} \text{ cm}^3/\text{s}$  [2]. Since the total rate constant for  $1S$ - $2S$  hyperfine-changing collisions is expected to be comparable to  $g$ , our results admit the possibility that  $1S$ - $2S$  excitation transfer collisions are much more probable than hyperfine-changing collisions. A first theoretical calculation of the relevant cross sections in this temperature regime is currently in progress [26].

## VI. CONCLUSION

In summary, we have completed the first determinations of loss rates due to inelastic collisions in a cold, trapped metastable H gas coexisting with a ground state background. The experimental values for the two-body loss rate  $K_2$  agree to order of magnitude ( $\sim 10^{-9} \text{ cm}^3/\text{s}$ ) with the present theory for  $2S$ - $2S$  collisions. Further refinements to the theory

will be necessary to explain an apparent increase in  $K_2$  with decreasing temperature below 230  $\mu\text{K}$ . Our metastable decay measurements also show that the total rate constant for inelastic  $1S$ - $2S$  collisions is not larger than  $\sim 10^{-13} \text{ cm}^3/\text{s}$  at the temperatures probed below 1 mK.

The present results pertain to total  $2S$ - $2S$  and  $1S$ - $2S$  inelastic collision rates. In future experiments with an enhanced Lyman- $\alpha$  detection efficiency and more complete suppression of stray electric fields, it may be possible to measure the rates due to excitation transfer processes alone by directly observing the fluorescence of  $2P$  states generated in collisions.

With the ability to create clouds of  $10^7$ - $10^8$  trapped metastables and a preliminary understanding of their inelastic collisions, the prospects are bright for fruitful new spectroscopic experiments involving the  $2S$  state. Recently, our group has performed spectroscopy of the H  $2S$ - $4P$  transition in a magnetic trap for the first time. Absorption spectroscopy on this and other single-photon transitions provide new tools for studying interactions of hydrogen states at low temperatures. It will also soon be possible to excite narrow two-photon transitions from the  $2S$  state, setting the stage for precision frequency measurements which probe fundamental physics.

#### ACKNOWLEDGMENTS

We are grateful to Alexander Dalgarno, Robert C. Forrey, Dale G. Fried, Piotr Froelich, and Thomas C. Killian for helpful conversations. We also thank Walter Joffrain for his assistance in the laboratory. This research was supported by the National Science Foundation and the Office of Naval Research.

## REFERENCES

\* Current address: Clarendon Photonics, 153 Needham St., Newton, MA 02464.

† Current address: Kernfysisch Versneller Instituut, Groningen, The Netherlands.

- [1] R. C. Forrey *et al.*, Phys. Rev. Lett. **85**, 4245 (2000).
- [2] H. T. C. Stoof, J. M. V. A. Koelman, and B. J. Verhaar, Phys. Rev. B **38**, 4688 (1988).
- [3] S. Jonsell *et al.*, Phys. Rev. A **65**, 042501 (2002).
- [4] M. J. Jamieson, A. Dalgarno, and J. M. Doyle, Mol. Phys. **87**, 817 (1996).
- [5] T. Udem *et al.*, Phys. Rev. Lett. **79**, 2646 (1997).
- [6] C. Schwob *et al.*, Phys. Rev. Lett. **82**, 4960 (1999).
- [7] M. Niering *et al.*, Phys. Rev. Lett. **84**, 5496 (2000).
- [8] L. Willmann and D. Kleppner, in *The Hydrogen Atom: Precision Physics of Simple Atomic Systems*, edited by S. G. Karshenboim *et al.* (Springer-Verlag, Berlin, 2001), p. 42.
- [9] M. Yasuda and F. Shimizu, Phys. Rev. Lett. **77**, 3090 (1996).
- [10] M. Morinaga *et al.*, Phys. Rev. Lett. **77**, 802 (1996).
- [11] A. Robert *et al.*, Science **292**, 461 (2001).
- [12] C. L. Cesar *et al.*, Phys. Rev. Lett. **77**, 255 (1996).
- [13] T. C. Killian *et al.*, Phys. Rev. Lett. **81**, 3807 (1998).
- [14] R. C. Forrey, S. Jonsell, A. Saenz, P. Froelich, and A. Dalgarno (submitted).
- [15] T. J. Greytak *et al.*, Physica B **280**, 20 (2000).
- [16] D. G. Fried *et al.*, Phys. Rev. Lett. **81**, 3811 (1998).
- [17] D. E. Pritchard, Phys. Rev. Lett. **51**, 1336 (1983).
- [18] H. F. Hess, Phys. Rev. B **34**, 3476 (1986).
- [19] D. E. Pritchard, K. Helmerson, and A. G. Martin, in *Atomic Physics 11*, edited by S. Haroche, J. C. Gay, and G. Grynberg (World Scientific, Singapore, 1989), p. 179.
- [20] H. A. Bethe and E. E. Salpeter, in *Quantum Mechanics of One- and Two-Electron Atoms* (Plenum, New York, 1977), p. 287.
- [21] D. Landhuis, Ph.D. thesis, Harvard University, 2002, arXiv.org/physics/0205054.
- [22] J. M. Doyle, Ph.D. thesis, Massachusetts Institute of Technology, 1991.
- [23] R. C. Forrey (private communication).
- [24] T. Orlikowski, G. Staszewska, and L. Wolniewicz, Molecular Physics **96**, 1445 (1999).
- [25] L. Willmann (in preparation).
- [26] B. Zygelman (in preparation).

## FIGURES

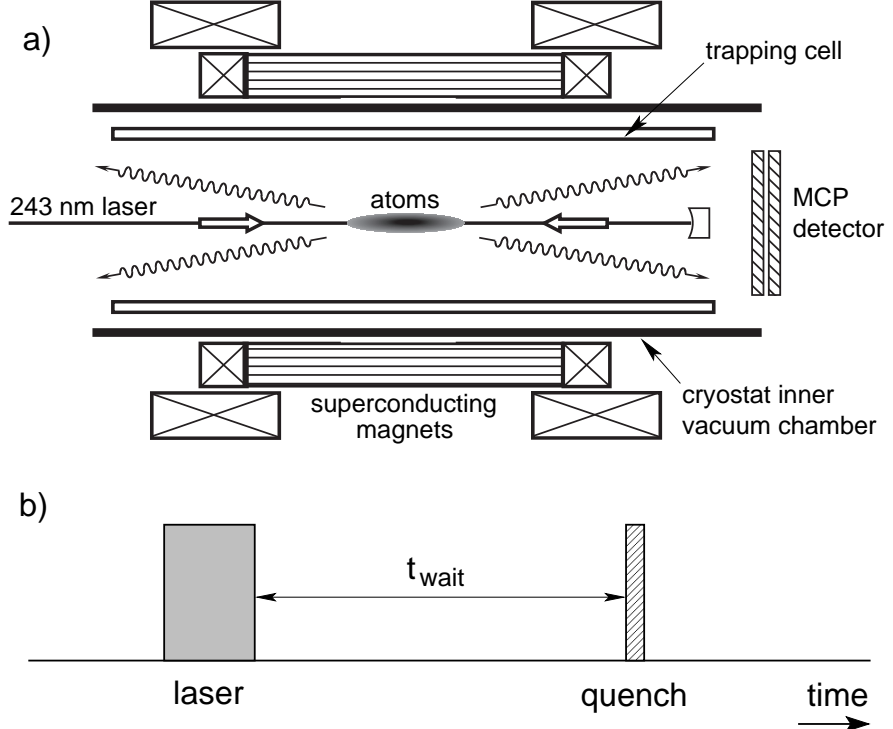


FIG. 1. (a) A schematic of the cryogenic trapping apparatus. Superconducting magnets produce the Ioffe-Pritchard trapping field. The UV excitation laser is reflected back on itself to permit Doppler-free two-photon excitation. The apparatus is roughly cylindrically symmetric about the trap axis, to which the laser is aligned. (b) Timing diagram for  $1S$ - $2S$  excitation spectroscopy. After a  $\sim 2$  ms excitation pulse and an additional time  $t_{\text{wait}}$ , the metastables are Stark-quenched by an electric field pulse, resulting in a burst of Lyman- $\alpha$  photons. In a typical decay measurement,  $t_{\text{wait}}$  is cycled through values between 1 and 92 ms.

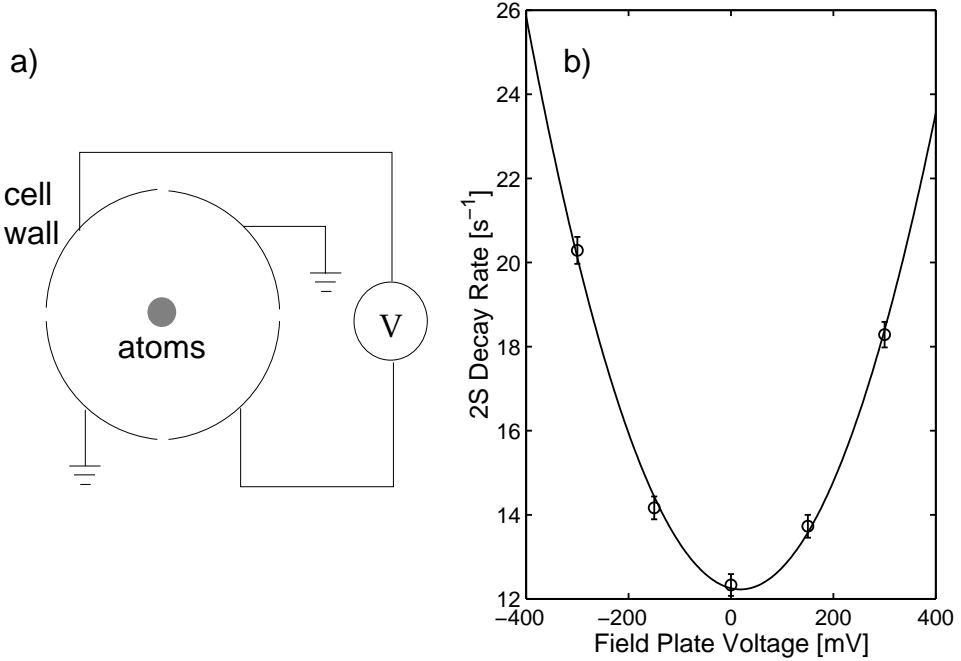


FIG. 2. (a) Schematic of trapping cell in cross section, showing electrical connections for the copper film electrodes used for both quenching and stray field compensation. The diameter of the trapping space is 4 cm. In the current design, compensation is possible for only one spatial direction. (b) Example of decay rate measurements for different applied dc fields for a single trapped sample. A parabola is fit to the data points, indicating the quadratic dependence of Stark quenching rate on the applied electric field.

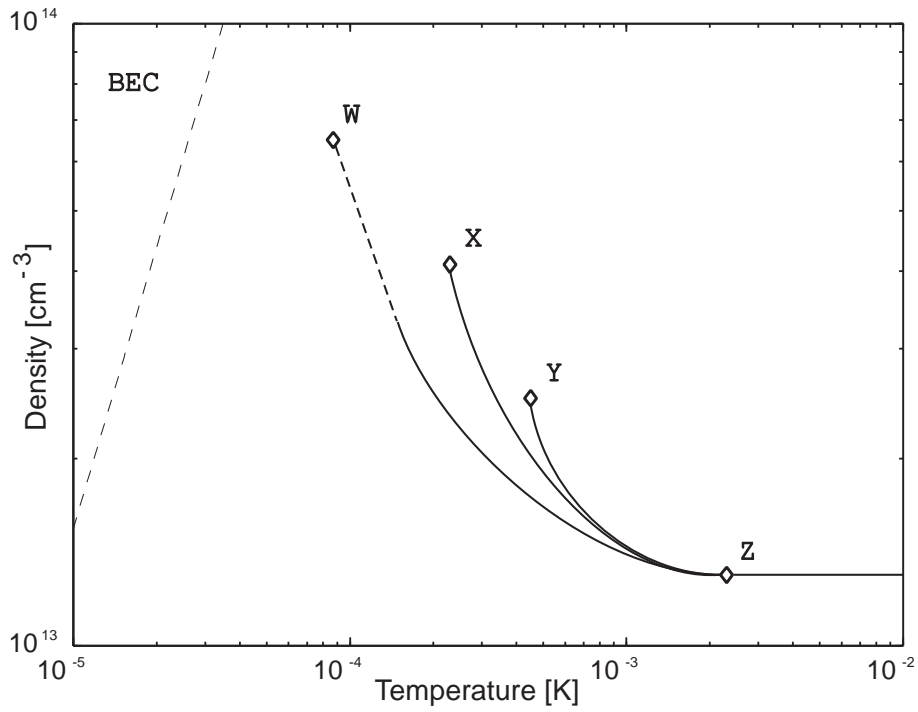


FIG. 3. Phase space plot of H samples used in metastable decay studies. “Density” is the peak initial ground state density prepared in the trap, and “Temperature” is the temperature of both ground state and metastable clouds. The approximate trajectory of the samples during magnetic saddlepoint evaporation is indicated by solid lines; for Trap W, a dashed line indicates the rf evaporation trajectory. A longer dashed line marks the boundary between the Bose-condensed (BEC) and normal phases of the gas.

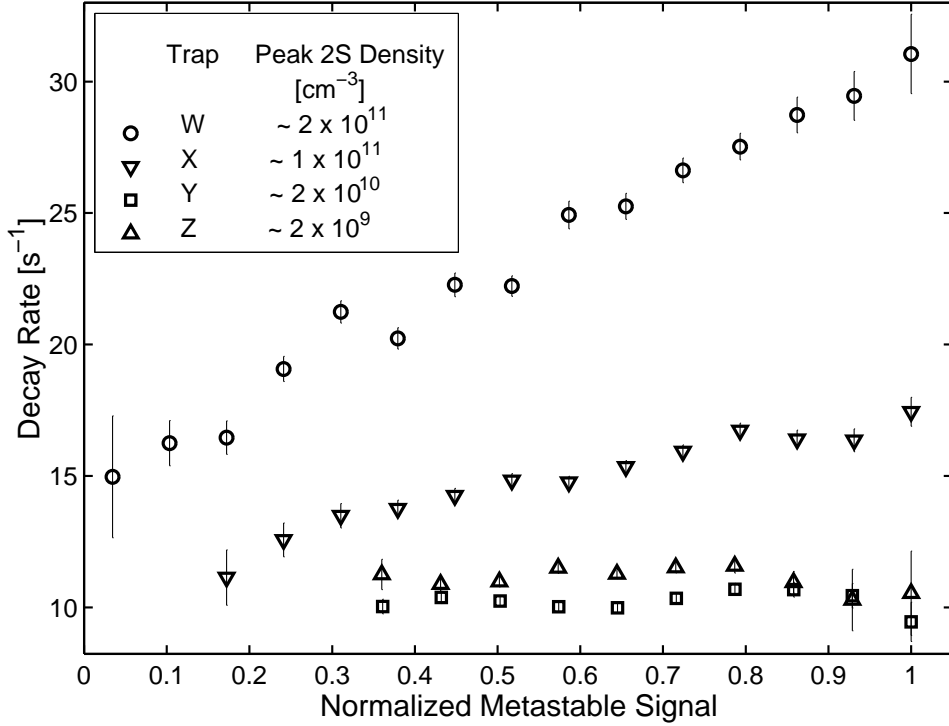


FIG. 4. Decay rates determined by exponential fits to decay curves recorded at different metastable signal levels in Traps W, X, Y, and Z. The bottom edge of the plot corresponds to the natural  $2S$  decay rate of  $8.2\text{ s}^{-1}$ , and the error bars are derived assuming only statistical uncertainty in the decay data. Different signal levels were achieved by varying the laser detuning and allowing the ground state sample to decay. The metastable signal, which is approximately proportional to the metastable density, has been normalized to the peak signal observed in each trap; estimates of the peak  $2S$  density corresponding to the peak signal are given in the legend. The metastable clouds produced in Traps W and X show a clear density dependence of the decay rate.

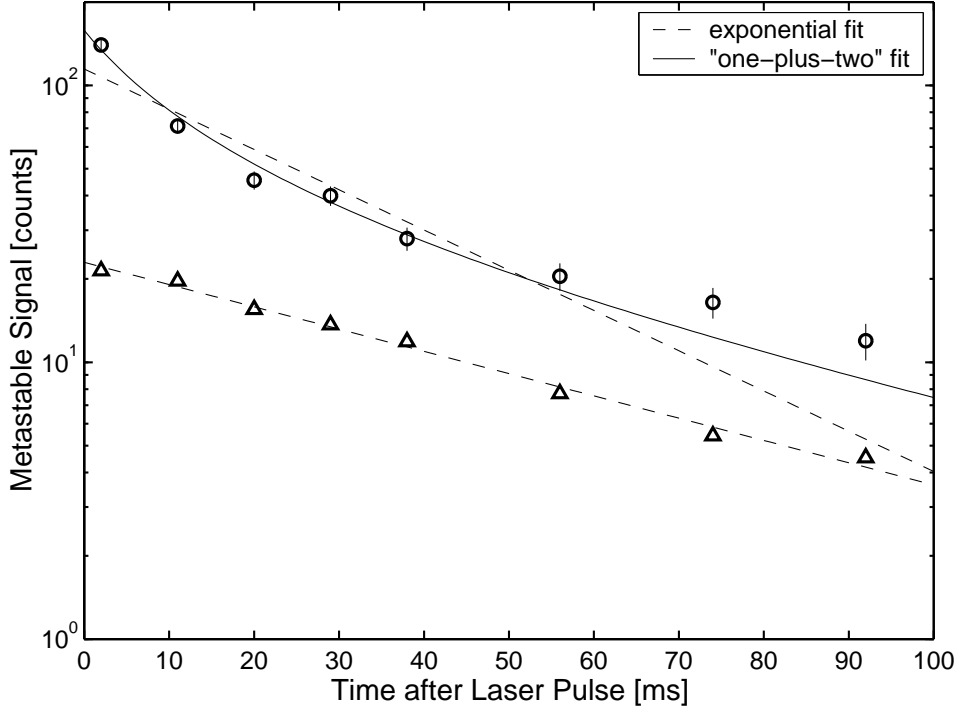


FIG. 5. Average decay curves for an initial  $2S$  density near the maximum achieved in Trap W (circles) and for an initial density in Trap W more than six times smaller (triangles). An exponential decay describes the low density data well, but the the high density data deviates significantly from the best fitting exponential decay. A simple “one-plus-two” model which has a fixed one-body decay parameter and a free two-body decay parameter fits the first  $\sim 50$  ms of the decay curve well. The model assumes a static cloud shape; in reality, the  $2S$  cloud changes shape as it decays, leading to deviation from the model at long wait times.

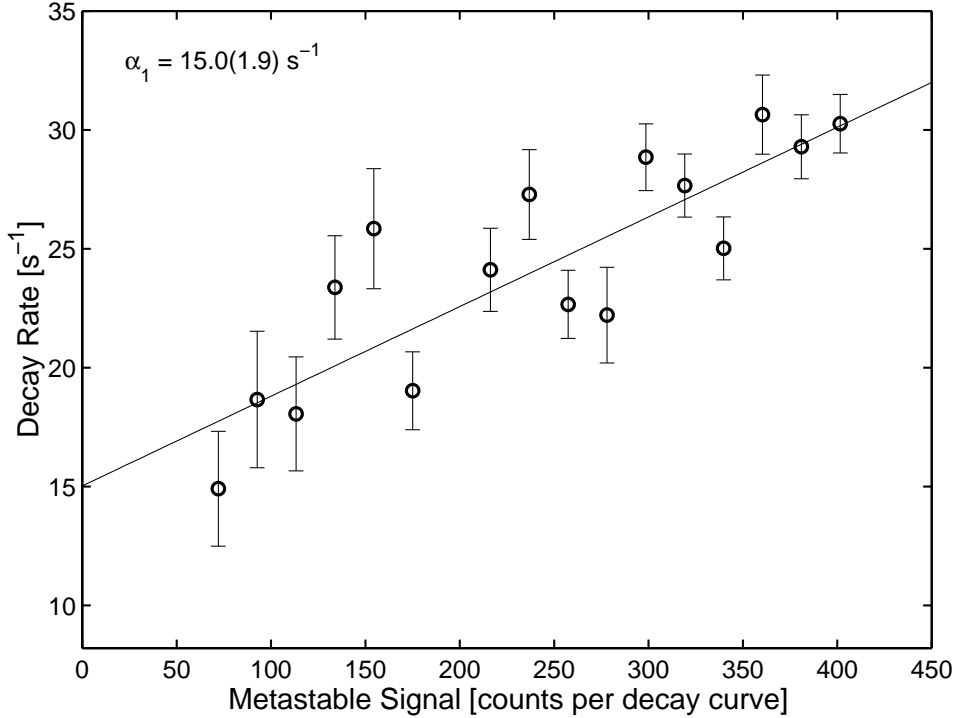


FIG. 6. Determination of  $\alpha_1$  by linear extrapolation of exponential decay rates to zero metastable signal. The decay data in this example was recorded in Trap W, and the bottom edge of the plot represents the natural decay rate. To avoid possible systematic errors due to a changing ground state density, the data set includes only those decay curves recorded in the first 9.6 s following excitation. The error bars on the decay rates assume only statistical errors in the decay curves; the uncertainty in  $\alpha_1$  is based on the scatter of decay rate values with respect to the linear fit.

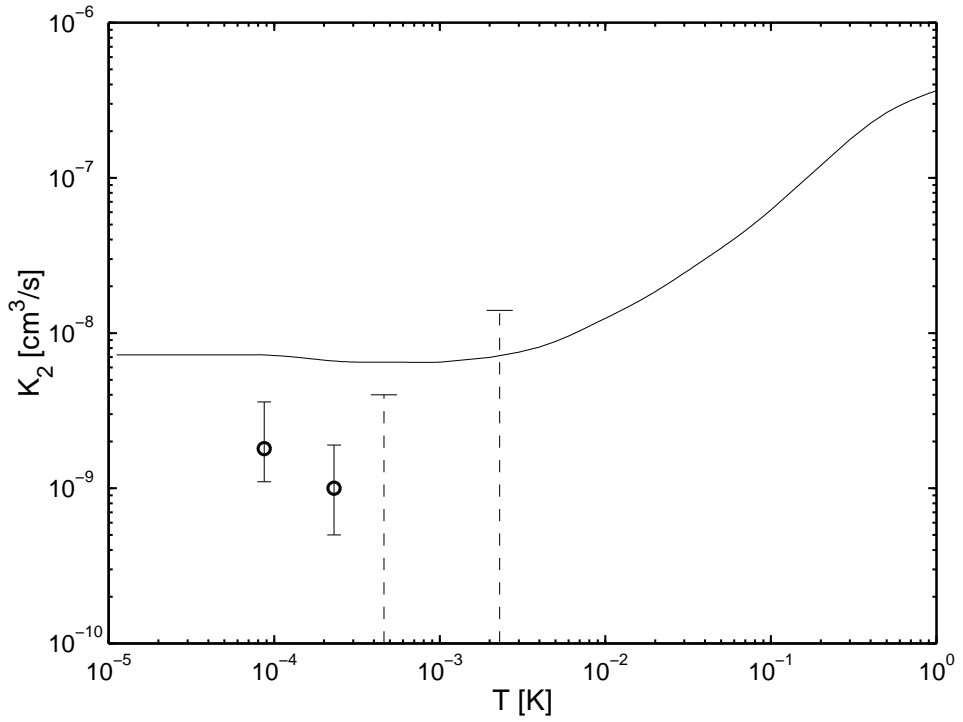


FIG. 7. Comparison of experimental results (circles) for  $K_2$  with the theoretical calculations (solid line) of Forrey and collaborators. At the temperatures where only upper limits were determined, dashed lines indicate the possible range of  $K_2$ . Since the uncertainties in the experimental points are highly correlated, the experimental results suggest that  $K_2$  has a significant temperature dependence below  $230 \mu\text{K}$ .

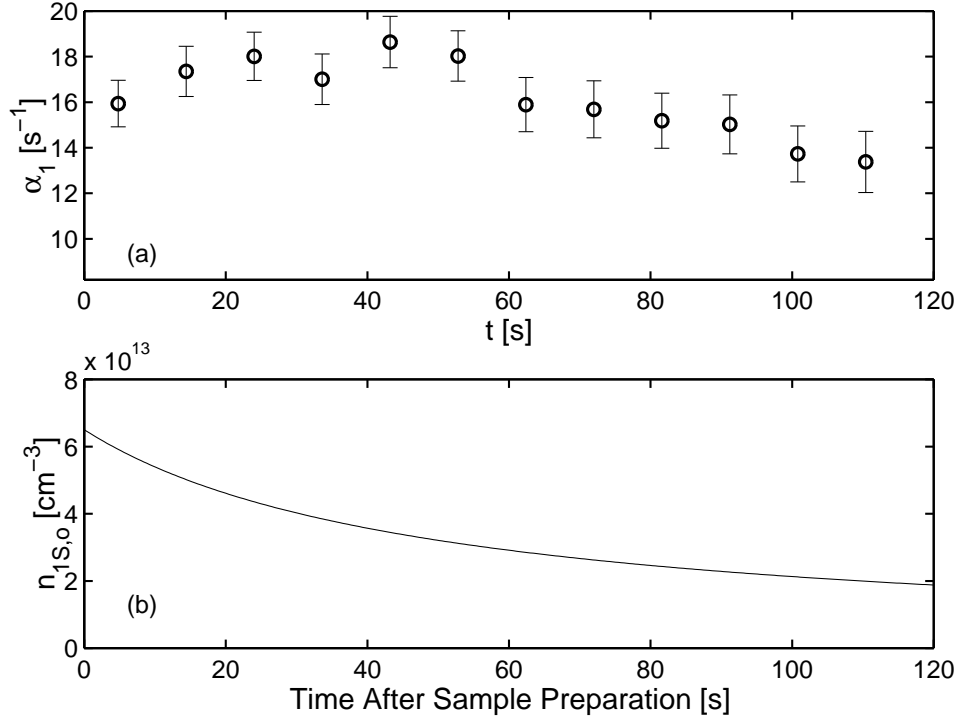


FIG. 8. (a) Weighted average of the one-body metastable loss rate  $\alpha_1$  as a function of time after preparation of the ground state sample in Trap W. The loss rate  $\alpha_1$  has been determined by extrapolation of exponential decay rates to zero metastable signal (see Fig. 6). The bottom edge of the plot corresponds to the natural decay rate, and error bars include only statistical uncertainties. (b) Peak 1S density calculated as a function of time in Trap W assuming that the only significant loss mechanism is 1S-1S dipolar decay. Comparison of (a) and (b) suggests that some of the one-body loss may be due to inelastic 1S-2S collisions.

## TABLES

| Trap | $T$ (mK) | Static approx.<br>$K_2$ ( $10^{-9}$ cm $^3$ /s) | With corrections<br>$K_2$ ( $10^{-9}$ cm $^3$ /s) |
|------|----------|---|---|
| W    | 0.087    | $1.4^{+1.3}_{-0.5}$                             | $1.8^{+1.8}_{-0.7}$                               |
| X    | 0.23     | $0.74^{+0.70}_{-0.35}$                          | $1.0^{+0.9}_{-0.5}$                               |
| Y    | 0.45     | $< 2$   | $< 4$   |
| Z    | 2.3      | $< 7$   | $< 14$  |

TABLE I. Results for  $K_2$  in the static approximation and including dynamic corrections. Sources of uncertainty are discussed in the text.

| Trap | $T$ (mK) | $K_{12}$ ( $10^{-13}$ cm $^3$ /s) |
|------|----------|-----------------------------------|
| W    | 0.087    | $< 5$                             |
| X    | 0.23     | $< 3$                             |
| Y    | 0.45     | $< 2$                             |
| Z    | 2.3      | $< 11$                            |

TABLE II. Experimental upper limits for  $K_{12}$  in the static approximation.